

Symmetry breaking and non-ergodicity in a driven-dissipative ensemble of multilevel atoms in a cavity

Enrique Hernandez ¹, Elmer Suarez ¹, Igor Lesanovsky ^{2,3}, Beatriz Olmos ²,
Philippe W. Courteille,⁴ and Sebastian Slama ^{5,*}

¹Center for Quantum Science and Physikalisches Institut, Eberhard-Karls Universität Tübingen,
Auf der Morgenstelle 14, 72076 Tübingen, Germany

²Institut für Theoretische Physik, Universität Tübingen, Auf der Morgenstelle 14, 72076 Tübingen, Germany

³School of Physics and Astronomy and Centre for the Mathematics and Theoretical Physics of Quantum Non-Equilibrium Systems,
The University of Nottingham, Nottingham NG7 2RD, United Kingdom

⁴Instituto de Física de São Carlos, Centro de Pesquisa em Óptica e Fotônica, Universidade de São Paulo,
Av. Trab. São Carlense 400, São Carlos, 13566-590 São Paulo, Brazil

⁵Center for Quantum Science and Physikalisches Institut, Eberhard-Karls Universität Tübingen,
Auf der Morgenstelle 14, 72076 Tübingen, Germany



(Received 28 May 2024; accepted 10 September 2024; published 26 September 2024)

Dissipative light-matter systems can display emergent collective behavior. Here, we report a \mathbb{Z}_2 -symmetry-breaking phase transition in a system of multilevel ^{87}Rb atoms strongly coupled to a weakly driven two-mode optical cavity. In the symmetry-broken phase, nonergodic dynamics manifests in the emergence of multiple stationary states with disjoint basins of attraction. This feature enables the amplification of a small atomic population imbalance into a characteristic macroscopic cavity transmission signal. Our experiment does not only showcase strongly dissipative atom-cavity systems as platforms for probing nontrivial collective many-body phenomena, but also highlights their potential for hosting technological applications in the context of sensing, density classification, and pattern retrieval dynamics within associative memories.

DOI: [10.1103/PhysRevResearch.6.L032072](https://doi.org/10.1103/PhysRevResearch.6.L032072)

Atom-cavity systems have been recently proposed as a platform for the observation of pattern retrieval dynamics [1,2], exploiting an intriguing link to the work by Hopfield on associative memories [3], and connecting to data classification in neural networks [4]. Learned patterns are encoded in the atom-light coupling constants. In the so-called pattern retrieval phase, the atomic ensemble dynamically evolves to the pattern that is closest to the initial state, i.e., the final state acts as an attractor for initial states located within its basin of attraction. This retrieval requires the breaking of ergodicity, i.e., a configuration space that decays into disconnected parts [5,6].

We demonstrate such pattern retrieval in a platform composed of an ensemble of multilevel atoms coupled to a pumped two-mode cavity [see Fig. 1(a)]. The system is strongly dissipative, i.e., the cavity modes and excited states are only weakly populated and can be adiabatically eliminated. Thus, the underlying nonlinearity is not based on saturation, nor on optomechanical effects, but on the existence of degenerate ground states [7]. While cavity QED systems are well established for studying static and dynamic

phase transitions [8–14], the inclusion of multiple ground states and degenerate cavity modes has recently attracted broad attention: transitions between different levels influence the collective coupling strength [15,16], and can thus lead to collective dark states [17,18], complex dynamical phenomena [19,20], photon-mediated interactions [21–23], and multistable states [24,25].

In our work the atomic multilevel structure interacting with more than a single cavity mode is key for the observed phenomena: A single mode can support a unique steady-state only [7]. We present evidence for a \mathbb{Z}_2 -symmetry-breaking dissipative phase transition by tuning the frequency of the driving laser field over the phase boundary. Nonergodic dynamics is observed in the symmetry-broken phase: here, the initial population determines the final state of the dynamics, corresponding to one out of several encoded patterns. Small population imbalances are amplified and converted into a macroscopic signal, allowing us to monitor the dynamics *in situ* by measuring the transmission of the cavity modes. This dynamical feature can be interpreted as pattern retrieval within an associative memory [3] or the solution of a density classification task [26]. The nonergodic behavior can, moreover, be utilized for quantum sensing applications, as recently demonstrated in Ref. [27].

Model. We consider an ensemble of N atoms with $2F + 1$ ground state levels, labeled by $m = -F, -F + 1, \dots, F$ and $2F' + 1$ excited state levels, labeled by $m' = -F', -F' + 1, \dots, F'$. The atoms interact with two circularly polarized modes of an optical cavity, represented by the creation and

*Contact author: sebastian.slama@uni-tuebingen.de

Published by the American Physical Society under the terms of the Creative Commons Attribution 4.0 International license. Further distribution of this work must maintain attribution to the author(s) and the published article's title, journal citation, and DOI.

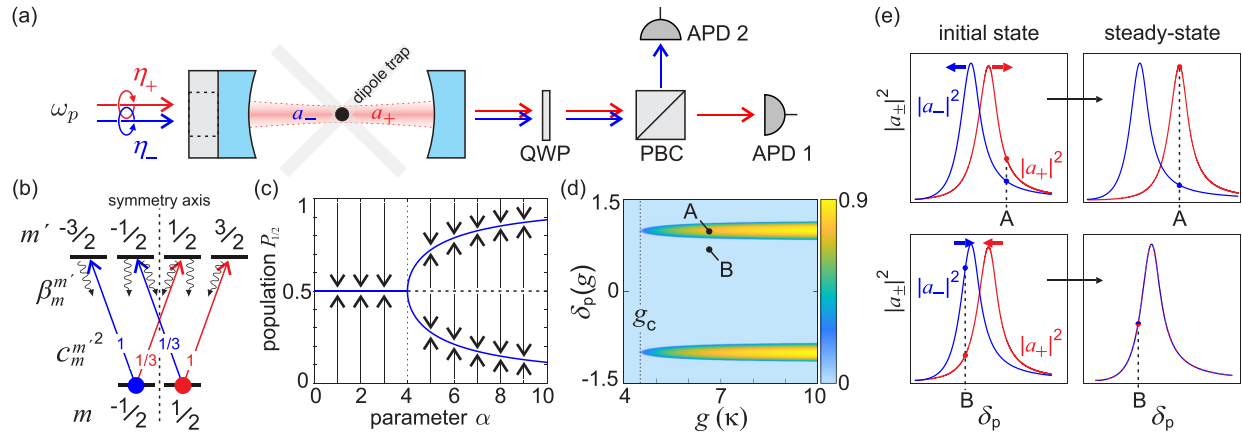


FIG. 1. *Physical model.* (a): Cold atoms in a cavity are pumped by two circularly polarized light beams, corresponding to cavity modes with fields a_{\pm} . The pump frequencies ω_p are detuned by δ_p from the empty cavity and atomic resonances. The transmission of the fields through the cavity is detected on two avalanche photo diodes (APD) after separation with a quarter wave plate (QWP) and a polarizing beam cube (PBC). (b): Simplified level scheme consisting of two ground states and four excited states with corresponding Clebsch Gordan coefficients $c_m^{m'}$ and atomic decay branching ratios $\beta_m^{m'}$. (c): Analytic solutions for $P_{1/2}$ (population of the $m = 1/2$ ground state) as a function of the parameter α . A symmetry-breaking phase occurs for $\alpha \geq 4$. The arrows indicate the basin of attraction to the stable solutions. (d): Population imbalance I_p vs the detuning δ_p and coupling strength g . A minimum coupling strength g_c is required to observe symmetry-breaking. (e): Each intracavity power $|a_{\pm}|^2$ shows a symmetric normal mode splitting around $\delta_p = 0$ (only $\delta_p > 0$ sketched). The initial splitting of the two modes depends of the initial atomic population imbalance (sketched $P_{1/2} > P_{-1/2}$). The choice of detuning determines whether in the steady state the population is imbalanced (upper row), or balanced (lower row).

annihilation bosonic operators a_l^\dagger and a_l with $l = \pm$, each of which are driven by a pump laser at a rate η_l and frequency ω_p , detuned by $\delta_p = \omega_p - \omega_a$ with respect to both cavity and atomic frequencies, $\omega_c = \omega_a$. As sketched in Fig. 1(b), the cavity modes a_+ (a_-) drive transitions between the ground state level m and the excited state $m' = m + 1$ ($m' = m - 1$). The Hamiltonian that describes the coherent dynamics can be decomposed into a sum $H = H_0 + H_{ia}$ of the independent cavity and atom evolution and the interaction between the two systems. In a frame rotating with the laser frequency, the independent Hamiltonian reads

$$H_0 = \hbar \sum_{l=\pm} [-\delta_p a_l^\dagger a_l + i\eta_l (a_l^\dagger - a_l)] - \hbar \delta_p \sum_{j=1}^N \sum_{ml} \sigma_{jm}^{m+l\dagger} \sigma_{jm}^{m+l}, \quad (1)$$

where we have introduced the atomic ladder operator $\sigma_{jm}^{m'} = |m\rangle_j \langle m'|$. After the rotating wave approximation, the interaction of the atoms with the two light fields is described by

$$H_{ia} = i\hbar \sum_{j=1}^N \sum_{ml} g_m^{m+l} (a_l^\dagger \sigma_{jm}^{m+l} - a_l \sigma_{jm}^{m+l\dagger}). \quad (2)$$

The interaction strength $g_m^{m'} = g_0 c_m^{m'}$, with atom-cavity coupling constant g_0 , depends on the transition via its corresponding Clebsch-Gordan coefficient $c_m^{m'\pm 1}$. Including the atomic and cavity field decay, the dynamics of the system is ultimately described by the quantum master equation

$$\begin{aligned} \dot{\rho} = & -\frac{i}{\hbar} [H, \rho] + 2\kappa \sum_l \left(a_l \rho a_l^\dagger - \frac{1}{2} \{a_l^\dagger a_l, \rho\} \right) \\ & + \Gamma \sum_{j=1}^N \sum_{mm'} \beta_m^{m'} \left(\sigma_{jm}^{m'} \rho \sigma_{jm}^{m'\dagger} - \frac{1}{2} \{ \sigma_{jm}^{m'\dagger} \sigma_{jm}^{m'}, \rho \} \right), \end{aligned} \quad (3)$$

where $\Gamma \beta_m^{m'}$ is the decay rate for each atom from level $|m'\rangle$ to $|m\rangle$ and 2κ the one of the cavity field. The master equation exhibits a \mathbb{Z}_2 -symmetry when $\eta_+ = \eta_-$, since the values of $\beta_m^{m'}$ and $g_m^{m'}$ are symmetric under the transformation $m \rightarrow -m$, $m' \rightarrow -m'$ and $l \rightarrow -l$ [see Fig. 1(b)].

Emergent collective dynamics. While Eq. (3) is valid for an arbitrary number of atomic levels, the essential features of the dynamics can be understood in the simple level scheme shown in Fig. 1(b) with $F = 1/2$ and $F' = 3/2$. Here, following the method outlined in Ref. [7] for a single mode cavity, we derive a rate equation for the two ground state populations $P_{\pm 1/2}$ in the weak pump limit. In this limit, the population of the excited states is negligible, a condition that is satisfied by the parameters of our experiment. For equal pumping, $\eta^2 = \eta_-^2 = \eta_+^2$, the rate equation is given by

$$\dot{P}_{1/2} = -\Gamma_{\text{eff}} [f(P_{1/2})P_{1/2} - f(P_{-1/2})(P_{-1/2})], \quad (4)$$

where $P_{1/2} + P_{-1/2} = 1$, and where the exact form of the effective decay rate $\Gamma_{\text{eff}} \propto \eta^2$ and nonlinear function f are given in the Supplemental Material [28]. Setting $\dot{P}_{1/2} = 0$ to find the steady state value of $P_{1/2}$ leads to the cubic equation

$$2\alpha P_{1/2}^3 - 3\alpha P_{1/2}^2 + (2 + \alpha)P_{1/2} - 1 = 0, \quad (5)$$

with a parameter α that depends on the pump detuning δ_p and on the (collective) coupling strength $g \equiv g_0 \sqrt{N}$. The parameter $\alpha(g, \delta_p)$ is a lengthy expression defined in the Supplemental Material [28]. In order to allow for a generalization to larger degeneracy of the ground state manifold we introduce the population imbalance $I_p = \sum_{m>0} P_m - \sum_{m<0} P_m$ as order parameter of the phase transition, which in case with two ground state levels is given by $I_p = P_{1/2} - P_{-1/2}$. The stable

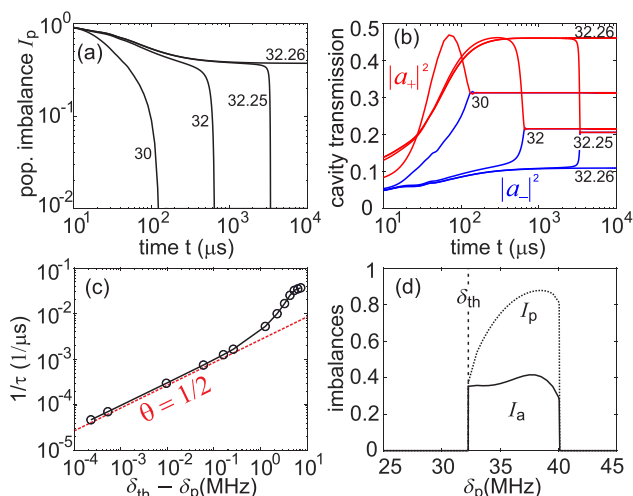


FIG. 2. *Simulation of the dynamics.* The initial conditions at $t = 0$ are $P_2 = 1$ and $P_m = 0$ for $m \neq 2$. Dynamics of (a): the population imbalance $I_p = P_2 + P_1 - P_{-1} - P_{-2}$ and (b): the intracavity power, for various values of detuning δ_p (in MHz). In the symmetry-broken regime, for $\delta_p > \delta_{th}$, at very long times the population imbalance remains $I_p \neq 0$ and the cavity fields do not reach the same value. (c): Close to the transition point $\delta_{th} - \delta_p \ll 1$ the relaxation time τ , defined here as the time it takes for I_p to decrease below 0.1, diverges algebraically with slope $\theta = 1/2$. (d): The symmetry-broken phase is characterized by a steady state imbalance of both the ground state populations I_p and the transmitted light power $I_a = |a_+|^2 - |a_-|^2$.

steady state solution of this parameter is given by

$$I_p = \begin{cases} 0 & \text{for } \alpha \leq 4, \\ \pm \sqrt{\frac{\alpha-4}{\alpha}} & \text{for } \alpha > 4, \end{cases} \quad (6)$$

i.e., a phase transition occurs at the critical point with $\alpha_c = 4$ from a symmetric phase with $P_{1/2} = P_{-1/2} = 1/2$ to a symmetry-broken phase, as one can observe in Fig. 1(c). A third unstable steady-state solution exists for $\alpha > 4$ with $\text{Re}[P_{1/2}] = 1/2$ and $\text{Im}[P_{1/2}] < 0$. Figure 1(d) shows that the symmetry-broken phase with $I_p \neq 0$ in the stationary state emerges in a frequency range around the normal mode splitting of the strongest transition, i.e., for $\delta_p \approx \pm g$, if the collective coupling strength exceeds a critical value of $g_c \approx 4.51\kappa$, with the number given by the Clebsch Gordan coefficients, see Supplemental Material [28].

This phase transition can be qualitatively understood in a simple picture sketched in Fig. 1(e), which shows the spectrum for each of the two modes. Importantly, the spectrum of each mode is split by the strong coupling between the cavity field and the atoms (only $\delta_p > 0$ of the splitting sketched in Fig. 2(e)). This so-called normal mode splitting depends on the populations of the ground state levels [14]. Any imbalance in the populations of levels $m = -1/2$ and $m = 1/2$ leads to a different normal mode splitting for each cavity mode. Thus, for a given fixed detuning δ_p , the intracavity photon numbers $|a_{\pm}|^2$ are in general different, despite equal pumping. Let us now for concreteness assume that initially there is a small excess of atoms in level $m = 1/2$, corresponding to the

splitting shown in the first column of Fig. 1(e). By choosing a detuning where $|a_+|^2 > |a_-|^2$ [first row in Fig. 1(e)], more atoms will then be pumped to $m = 1/2$. Thus, the normal mode splitting of level $m = 1/2$, i.e., $|a_+|^2$, increases, and that of level $m = -1/2$, $|a_-|^2$, decreases. This further enhances the pumping to level $m = 1/2$, which becomes a runaway process and increases in turn the population imbalance. This dynamic thus features (i) symmetry-breaking: the initial condition selects which stationary state is chosen, and (ii) leads to density classification: small population imbalances are growing, accompanied by a characteristic change of the cavity transmission. Thus, we can determine population imbalances by observing the light transmitted through the cavity, without the need to directly measure the state of the atoms. If, on the other hand, the detuning is set to a value where $|a_-|^2 > |a_+|^2$ [second row in Fig. 1(e)], more atoms are pumped to $m = -1/2$, thereby decreasing the excess of population. As the same argument holds for an excess of atoms in $m = -1/2$, the dynamics will approach a steady state with equal populations where $I_p = 0$, and no ergodicity-breaking is observed.

Universal features. In the following we investigate the universal properties of the phase transition, with the main results summarized here while details are found in the Supplemental Material [28]. The population imbalance I_p near the transition point at $\alpha_c = 4$ can be written as $I_p \sim \pm(\alpha - \alpha_c)^\beta$, with critical exponent $\beta = 1/2$. This is the same scaling behavior as the one observed in the mean-field Ising model with vanishing magnetic field H , where the magnetization scales like $M(T, H = 0) = |T - T_c|^\beta$, with temperature T and critical temperature T_c [29]. When weakly perturbing the system near the critical point, it relaxes to stationarity via a power-law behavior: indeed, for $\alpha = \alpha_c$ small imbalances return to the steady state as $I_p \sim (\Gamma_{\text{eff}} t)^{-1/\zeta}$, with critical exponent $\zeta = 2$. Finally, introducing an external field $\Delta\eta$ that breaks the symmetry of the two stable solutions by the relative imbalance in the pumping rates, $\Delta\eta = (\eta_+^2 - \eta_-^2)/\eta_-^2$, we obtain that the resulting imbalance scales as $I_p \sim \Delta\eta^{1/\delta}$, with critical exponent $\delta = 3$. We conclude that for two ground states the universality class associated with the phase transition is the same as the one of the mean-field Ising model.

Numerical simulation. We consider now a more complex case, where each atom has five and seven ground and excited state levels, respectively ($F = 2$ and $F' = 3$), which reflects the situation in our experiment. The level scheme, including the values of $c_m^{m'}$ and $\beta_m^{m'}$, is given in the Supplemental Material [28]. Here, the large amount of twelve coupled levels makes deriving and analyzing closed equations such as Eq. (4) infeasible. We use instead a fully numerical approach: we derive and solve the mean-field Heisenberg equations of motion starting from the master equation (3) with help of the QUANTUMCUMULANTS package of the Julia software [30]. Thus, plotted simulation results show expectation values of the operators. The pumping strength is chosen as $\eta_+ = \eta_- = 14\kappa$, which is large enough to keep the simulations fast, and small enough to avoid saturation of the atoms (excited state population stays well below 1% for all times). The initial populations are set to $P_2 = 1$ and $P_m = 0$ for $m \neq 2$ to put the system in the maximally imbalanced state. The Heisenberg equations are numerically integrated to obtain the time evolution until the steady state is reached. Results are

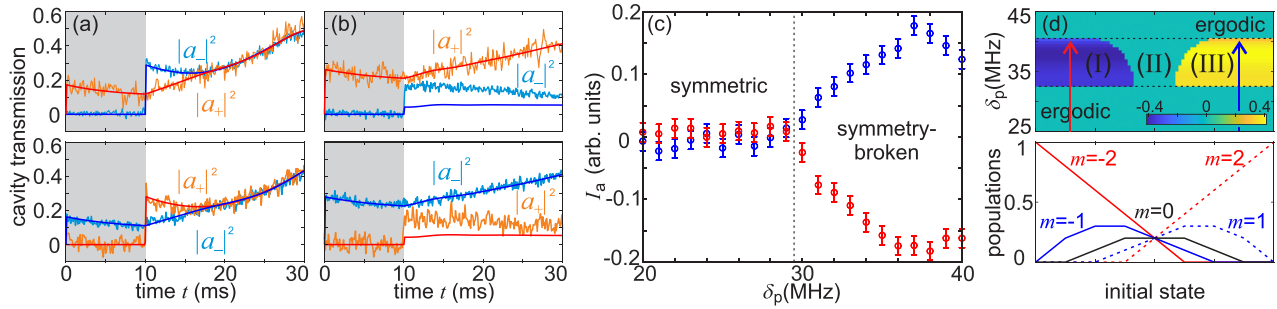


FIG. 3. *Symmetry breaking.* Cavity transmission in the symmetric phase for (a): $\delta_p = 23$ MHz, and within the symmetry-broken phase for (b): $\delta_p = 33$ MHz, and comparison with simulations (solid lines). The populations are prepared in an unbalanced state by 10 ms of initial pumping (grey shaded area). Top and bottom subfigures correspond to an inverted time sequence of the pump beams. In (a) the final state does not depend on the initial conditions whereas in (b) the ergodicity is broken and the system evolves to one of the two solutions, depending on the time sequence. (c): Cavity field imbalance I_a measured at $t = 20$ ms as a function of the detuning, where the transition from the symmetric to the symmetry-broken phase is clearly visible at $\delta_p \approx 30$ MHz. Blue and red data correspond to an inverted pump time sequence. (d): The upper panel shows the numerically simulated I_a as a function of the detuning δ_p and the initial populations P_m , shown in the lower panel. Unlike for the simple model with only two ground states, configuration space in the symmetry-broken phase decays into three basins of attraction (I) to (III), as indicated also by the colors. The red and blue arrow indicate the directions along which we experimentally probe the phase transition in (c).

shown in Figs. 2(a) and 2(b) for the population imbalance $I_p = P_2 + P_1 - P_{-1} - P_{-2}$ and cavity transmission $|a_{\pm}|^2$, respectively, for different values of the detuning δ_p . In order to match with our experimental parameters, we have used following numbers in the simulations: cavity field decay rate $\kappa = 2\pi \times 6$ MHz, atomic decay rate $\Gamma = \kappa$, $g_0 = 0.0654 \kappa$, and atom number $N = 20000$. We observe that for all values of δ_p smaller than a threshold at $\delta_{th} \approx 32.259$ MHz the imbalance both in atomic population and cavity transmission eventually reaches a value of zero, while for $\delta_p \gtrsim \delta_{th}$ the imbalance persists in both quantities for all times. Close to the phase transition, a metastable plateau is observed [29]. Figure 2(c) shows that the time τ it takes until the imbalance vanishes diverges algebraically at the phase transition, i.e., $1/\tau \propto (\delta_{th} - \delta_p)^\theta$ with exponent $\theta = 1/2$. These results are summarized in Fig. 2(d), where we clearly identify the symmetry-broken region as the detuning changes.

Experimental results. To probe the phase transition and ergodicity-breaking behavior we use ultracold ^{87}Rb atoms, which are cooled in a magneto-optic trap and loaded into a crossed beam optical dipole trap. Thus, we prepare a number of $N = 20000$ atoms at a temperature of $T = 20 \mu\text{K}$ in the mode volume of an optical cavity with field decay rate $\kappa = 2\pi \times 6$ MHz and coupling constant $g_0 = 0.0654 \kappa$. The cavity is then pumped with circularly polarized light fields, near resonant to the D2 line at $\lambda = 780$ nm, as depicted in Fig. 1(a). Thus, the collective coupling strength is $g = 2\pi \times 28$ MHz for the stretched transition. The transmissions behind the cavity are separated by polarizations optics and detected using APDs. Further details on the experimental setup are described in the Supplemental Material [28]. We initially prepare ground state populations with some imbalance by 10 ms of optical pumping with only one of the two cavity fields. After the pumping, the second cavity field is switched on with equal pump strength, i.e., $\eta_+ = \eta_-$, and we observe the dynamics of the transmitted light powers on the corresponding APDs. We detail two typical measurements within and outside the symmetry-broken regime and focus on

the first 30 ms, where the signatures of the different phases become apparent. Additional measurements at more detunings and for longer times are shown in the Supplemental Material [28]. Deviations between the experimental data and simulations are caused by the scaling of the cavity transmission, as explained also in the Supplemental Material [28]. Here, Figs. 3(a) and 3(b) show the dynamics within the symmetric phase and the symmetry-broken regime, respectively. The smoking gun for symmetry-breaking is here the observation that the transmission curves do not tend to the same value. Instead, further separating transmissions show that the initially prepared asymmetry is increasing. Top and bottom subfigures show the dynamics when the time sequence of the two pumps is inverted, such that the initial population at $t = 10$ ms is imbalanced in favor of states with $m < 2$ or $m > 2$, respectively. This has no effect on the steady state in the symmetric phase. In contrast, in the symmetry-broken phase the subsequent dynamics is exchanged, signaling the breaking of ergodicity.

The phase transition also manifests in the imbalance $I_a = |a_+|^2 - |a_-|^2$ of the cavity fields at long times as shown by the experimental data displayed in Fig. 3(c) as a function of the detuning. We have chosen a time of $t = 20$ ms for this analysis, where pumping in the symmetric phase is mostly finished, and the effect of atom loss is still negligible. We observe a nonzero imbalance for detunings $\delta_p \gtrsim 30$ MHz, whose sign depends on the order of the pump time sequence. Determining the value of the threshold more precisely is prevented by the divergence of time scales close to the phase transition and the subsequent influence of atom losses: Here, starting in the symmetric phase closely below the threshold, atom losses can cause the transition into the symmetry-broken phase and vice versa as the reduction of N leads to a decreased $g = g_0\sqrt{N}$, as shown in the Supplemental Material [28]. Figure 3(d) shows the simulated field imbalance I_a in the steady state as function of the detuning for various initial populations. To simplify the analysis, we project the four-dimensional parameter space of the ground-state levels to a line (plotted on the lower axis)

that connects the fully stretched states and contains the state with equal populations at its center. We observe again that, for a certain range of detunings, ergodicity is broken. In the previously considered case of atoms with two ground states, three stationary states exist out of which, however, only two are stable [Fig. 1(c)]. Here, conversely, as shown in Fig. 3(d), three different stable basins of attraction, labeled (I) to (III) exist, and the initial conditions determine which one of the stationary states is reached. This is reminiscent of the multicritical Ising model, which is discussed in Ref. [31], and suggests that the transition between symmetric and symmetry-broken phase may be governed by a different universality class. We plan to explore the phase diagram of this system in more detail in future work.

Conclusion. We have observed a symmetry-breaking phase transition in a strongly dissipative system composed of a driven two-mode cavity and an ensemble of multilevel atoms. In the symmetry-broken phase, several stationary states exist each with their own basin of attraction. This setting bears close resemblance with density classification dynamics, or pattern retrieval within a Hopfield associative memory. In this context, it would be interesting to move away from the

strongly dissipative limit and explore a parameter space with larger numbers of steady-states, as provided by higher coupling strength [25]. This is expected to lead to the emergence of new (quantum) patterns which have been predicted in quantum generalized Hopfield neural networks [32]. Moreover, multistate atoms allow to engineer and probe even more exotic models, such as quantum generalized Potts-Hopfield neural networks [33].

Acknowledgments. The project was funded by the Deutsche Forschungsgemeinschaft (DFG, German Research Foundation) - 422447846 and 465199066. It was carried out within research unit FOR 5413 “Long-range interacting quantum spin systems out of equilibrium: Experiment, Theory and Mathematics”. I.L. further acknowledges funding through the Deutsche Forschungsgemeinschaft (DFG, German Research Foundation), through Project No. 449905436 and the Machine Learning Cluster of Excellence under Germany’s Excellence Strategy — EXC number 2064/1 – Project No. 390727645. We acknowledge support from the Open Access Publication Fund of the University of Tübingen. We thank H. Ritsch and C. Hotter for support with the QUANTUMCUMULANTS package in Julia.

-
- [1] F. Carollo and I. Lesanovsky, Exactness of mean-field equations for open Dicke models with an application to pattern retrieval dynamics, *Phys. Rev. Lett.* **126**, 230601 (2021).
- [2] B. P. Marsh, Y. Guo, R. M. Kroeze, S. Gopalakrishnan, S. Ganguli, J. Keeling, and B. L. Lev, Enhancing associative memory recall and storage capacity using confocal cavity QED, *Phys. Rev. X* **11**, 021048 (2021).
- [3] J. J. Hopfield, Neural networks and physical systems with emergent collective computational abilities, *Proc. Natl. Acad. Sci. USA* **79**, 2554 (1982).
- [4] S. Gopalakrishnan, B. L. Lev, and P. M. Goldbart, Frustration and glassiness in spin models with cavity-mediated interactions, *Phys. Rev. Lett.* **107**, 277201 (2011).
- [5] E. Fiorelli, M. Marcuzzi, P. Rotondo, F. Carollo, and I. Lesanovsky, Signatures of associative memory behavior in a multimode Dicke model, *Phys. Rev. Lett.* **125**, 070604 (2020).
- [6] B. P. Marsh, R. M. Kroeze, S. Ganguli, S. Gopalakrishnan, J. Keeling, and B. L. Lev, Entanglement and replica symmetry breaking in a driven-dissipative quantum spin glass, *Phys. Rev. X* **14**, 011026 (2024).
- [7] E. Suarez, F. Carollo, I. Lesanovsky, B. Olmos, P. W. Courteille, and S. Slama, Collective atom-cavity coupling and nonlinear dynamics with atoms with multilevel ground states, *Phys. Rev. A* **107**, 023714 (2023).
- [8] S. Slama, S. Bux, G. Krenz, C. Zimmermann, and P. W. Courteille, Superradiant Rayleigh scattering and collective atomic recoil lasing in a ring cavity, *Phys. Rev. Lett.* **98**, 053603 (2007).
- [9] K. Baumann, C. Guerlin, F. Brennecke, and T. Esslinger, Dicke quantum phase transition with a superfluid gas in an optical cavity, *Nature (London)* **464**, 1301 (2010).
- [10] R. M. Kroeze, Y. Guo, V. D. Vaidya, J. Keeling, and B. L. Lev, Spinor self-ordering of a quantum gas in a cavity, *Phys. Rev. Lett.* **121**, 163601 (2018).
- [11] E. J. Davis, A. Periwal, E. S. Cooper, G. Bentsen, S. J. Evered, K. Van Kirk, and M. H. Schleier-Smith, Protecting spin coherence in a tunable Heisenberg model, *Phys. Rev. Lett.* **125**, 060402 (2020).
- [12] S. C. Schuster, P. Wolf, S. Ostermann, S. Slama, and C. Zimmermann, Supersolid properties of a Bose-Einstein condensate in a ring resonator, *Phys. Rev. Lett.* **124**, 143602 (2020).
- [13] H. Keßler, P. Kongkhambut, C. Georges, L. Mathey, J. G. Cosme, and A. Hemmerich, Observation of a dissipative time crystal, *Phys. Rev. Lett.* **127**, 043602 (2021).
- [14] T. D. F. Mivehvar, F. Piazza and H. Ritsch, Cavity QED with quantum gases: New paradigms in many-body physics, *Adv. Phys.* **70**, 1 (2021).
- [15] K. M. Birnbaum, A. S. Parkins, and H. J. Kimble, Cavity QED with multiple hyperfine levels, *Phys. Rev. A* **74**, 063802 (2006).
- [16] K. J. Arnold, M. P. Baden, and M. D. Barrett, Collective cavity quantum electrodynamics with multiple atomic levels, *Phys. Rev. A* **84**, 033843 (2011).
- [17] A. P. Orioli, J. K. Thompson, and A. M. Rey, Emergent dark states from superradiant dynamics in multilevel atoms in a cavity, *Phys. Rev. X* **12**, 011054 (2022).
- [18] B. Sundar, D. Barbarena, A. M. Rey, and A. P. Orioli, Squeezing multilevel atoms in dark states via cavity superradiance, *Phys. Rev. Lett.* **132**, 033601 (2024).
- [19] A. Chu, A. P. Orioli, D. Barbarena, J. K. Thompson, and A. M. Rey, Photon-mediated correlated hopping in a synthetic ladder, *Phys. Rev. Res.* **5**, L022034 (2023).
- [20] R. J. Valencia-Tortora, S. P. Kelly, T. Donner, G. Morigi, R. Fazio, and J. Marino, Crafting the dynamical structure of synchronization by harnessing bosonic multilevel cavity QED, *Phys. Rev. Res.* **5**, 023112 (2023).
- [21] P. Samutpraphoot, T. Đorđević, P. L. Ocola, H. Bernien, C. Senko, V. Vuletić, and M. D. Lukin, Strong coupling of two individually controlled atoms via a nanophotonic cavity, *Phys. Rev. Lett.* **124**, 063602 (2020).
- [22] T. W. Clark, A. Dombi, F. I. B. Williams, A. Kurko, J. Fortagh, D. Nagy, A. Vukics, and P. Domokos, Time-resolved

- observation of a dynamical phase transition of atoms in a cavity, *Phys. Rev. A* **105**, 063712 (2022).
- [23] B. Gabor, D. Nagy, A. Dombi, T. W. Clark, F. I. B. Williams, K. V. Adwaith, A. Vukics, and P. Domokos, Ground state bistability of cold atoms in a cavity, *Phys. Rev. A* **107**, 023713 (2023).
- [24] F. Ferri, R. Rosa-Medina, F. Finger, N. Dogra, M. Soriente, O. Zilberberg, T. Donner, and T. Esslinger, Emerging dissipative phases in a superradiant quantum gas with tunable decay, *Phys. Rev. X* **11**, 041046 (2021).
- [25] B. Gabor, D. Nagy, A. Vukics, and P. Domokos, Quantum bistability in the hyperfine ground state of atoms, *Phys. Rev. Res.* **5**, L042038 (2023).
- [26] M. Land and R. K. Belew, No perfect two-state cellular automata for density classification exists, *Phys. Rev. Lett.* **74**, 5148 (1995).
- [27] D.-S. Ding, Z.-K. Liu, B.-S. Shi, G.-C. Guo, K. Mølmer, and C. S. Adams, Enhanced metrology at the critical point of a many-body Rydberg atomic system, *Nat. Phys.* **18**, 1447 (2022).
- [28] See Supplemental Material at <http://link.aps.org/supplemental/10.1103/PhysRevResearch.6.L032072> for derivation of the rate equation and universal features, experimental details, data evaluation, fit parameters, and additional measurements.
- [29] M. Marcuzzi, E. Levi, S. Diehl, J. P. Garrahan, and I. Lesanovsky, Universal nonequilibrium properties of dissipative Rydberg gases, *Phys. Rev. Lett.* **113**, 210401 (2014).
- [30] D. Plankensteiner, C. Hotter, and H. Ritsch, QuantumCumulants.jl: A Julia framework for generalized mean-field equations in open quantum systems, *Quantum* **6**, 617 (2022).
- [31] V. R. Overbeck, M. F. Maghrebi, A. V. Gorshkov, and H. Weimer, Multicritical behavior in dissipative Ising models, *Phys. Rev. A* **95**, 042133 (2017).
- [32] P. Rotondo, M. Marcuzzi, J. P. Garrahan, I. Lesanovsky, and M. Müller, Open quantum generalisation of Hopfield neural networks, *J. Phys. A: Math. Theor.* **51**, 115301 (2018).
- [33] E. Fiorelli, I. Lesanovsky, and M. Müller, Phase diagram of quantum generalized Potts-Hopfield neural networks, *New J. Phys.* **24**, 033012 (2022).